universe

MDPI

Article

Dynamics of a Cosmological Model in $f(R,T)$ Gravity: I. On Invariant Planes

Jianwen Liu, Ruifang Wang and Fabao Gao *

School of Mathematical Science, Yangzhou University, Yangzhou 225002, China; liuweniie@163.com (J.L.); wangruifang16@sina.com (R.W.)

* Correspondence: gaofabao@sina.com or fbgao@yzu.edu.cn

Abstract: Under the background of perfect fluid and flat Friedmann–Lemaître–Robertson–Walker (FLRW) space-time, this paper mainly describes the dynamics of the cosmological model constructed in $f(R,T)$ gravity on three invariant planes, by using the singularity theory and Poincaré compactification in differential equations.

Keywords: dynamics; $f(R,T)$ gravity; invariant plane; FLRW metric; Poincaré compactification

check for updates

Citation: Liu, J.; Wang, R.; Gao, F. Dynamics of a Cosmological Model in $f(R,T)$ Gravity: I. On Invariant Planes. *Universe* **2022**, *8*, 365. https://doi.org/10.3390/universe8070365

Academic Editor: Sergei D. Odintsov

Received: 20 May 2022
Accepted: 30 June 2022
Published: 3 July 2022

1. Introduction

General Relativity (GR) is one of the pillars of modern physics, known as the standard model of gravitation and cosmology, with many successes [1–3]. However, the theory in its usual form fails to explain the late-time acceleration observed experimentally in high redshift supernova [4,5]. Furthermore, GR cannot match with quantum theory and explain the flatness of galaxy rotation curves [6,7]. To this end, scientists have proposed many novel ideas to overcome different aspects of its incompleteness and shortcomings. Some of these ideas modify or generalize GR in a geometrical background. Other ideas introduce new cosmic fluids, such as dark matter, responsible for clustering galaxy structures and dark energy that accelerates the observed accelerating expansion of the Universe. The former has attracted a great deal of interest in recent years. Many researchers have proposed more complicated gravity theories in which high-order curvature invariants correct for the Einstein–Hilbert action concerning the Ricci scalar.

In higher-order gravitational theory, a simple modification is the $f(R)$ theory of gravity, obtained by substituting the Ricci scalar R with an arbitrary function in the Einstein–Hilbert action. In some cases, the theory can solve specific problems [8–10] and predict a comparison of the early accelerated expansion of the Universe with the late-time accelerated expansion, matching observational cosmology data [11–14]. Some researchers tested the viability of $f(R)$ gravity models to explain dark energy and later-time Universe [15–17]. It has been observed that the conclusions of the models in $f(R)$ gravity which accounts for the local gravity and cosmic problems are different from those of the ΛCDM model [18]. Two feasible models of $f(R)$ gravity in Palatini formalism and the properties of geometric dark energy in modified gravity were recently investigated in [19], and it was concluded that the ΛCDM model was the best fit for the current data. A generalization of the $f(R)$ theory has been proposed [20] by introducing an explicit coupling of an arbitrary function of the Ricci scalar R to the matter Lagrangian density L_{m} in theory. Harko [21] obtained a maximal extension of the Lagrangian by considering the Einstein–Hilbert Lagrangian as a general function of R and L_{m}. In $f(R,L_{\mathrm{m}})$ gravity, it is assumed that the matter Lagrangian L_{m} contains all the properties of matter, which was generalized to any coupling between matter and geometry [22].

In 2011, Harko et al. proposed a new modified theory of gravity known as $f(R,T)$ gravity [23], which is considered a generalization of $f(R)$ gravity as it incorporates the Ricci scalar R and the trace of the energy-momentum tensor T. The primary justification for the dependence on trace T may be induced by the existence of some imperfect exotic fluid or quantum effects originating from a conformal anomaly trace. The dynamical and gravitation equations were developed for test particles, and higher-curvature theories were found to help to resolve the flat problem in galaxies' rotation curves. In the $f(R,T)$ theory of gravity, cosmic acceleration depends on geometrical contribution to the total cosmic energy density and on matter particles. Since the birth of this theory, its various aspects have been investigated, such as dark energy [24], dark matter [25], redshift drift [26], wormholes [27,28], thermodynamics [29,30], bouncing cosmology [31,32], baryogenesis [33], scalar perturbations [34], gravitational waves [35,36]. The reconstruction schemes of the $f(R,T)$ theory were investigated in [37–39]. Shabani and Farhoudi [40,41] studied different types of $f(R,T)$ cosmological models with miscellaneous cosmological quantities by applying a dynamical system approach. Baffou et al. [42] studied the dynamics and stability of the model obtained by imposing the conservation of the energy momentum tensor. The model can be regarded as a potential dark energy candidate. Sharma and Pradhan [43] presented an analysis of cosmological solution in modified $f(R,T)$ theory with $\Lambda(T)$. The late-time dynamics of a complete form of the $f(R,T)$ gravity were investigated in [44], and their results are consistent with standard cosmology. Other relevant literature can be referred to [45,46].

Dynamical system analysis is a powerful mathematical tool for studying the dynamical behavior of models of the universe without analytically solving field equations. This method has been used for a broad class of models in different gravity theories [47–50]. Equilibrium points in the governing equations of cosmological models can describe different epochs of the universe. Considering the perfect fluid and flat FLRW space-time, this study will investigate the dynamics (including the infinite case) and cosmological evolution of the $f(R,T) = \xi R^{\alpha} + \zeta\sqrt{-T}$ gravitational model on invariant planes by the dynamical system analysis method. To capture all possible equilibrium points near infinity, the Poincaré compactification method is usually applied, which maps all infinity points to points on the boundary of the Poincaré sphere. The involved singularity theory accurately computes trajectories around some unusual equilibrium points. The stability of all equilibrium points is discussed to draw phase diagrams for different invariant planes. Furthermore, we study the case $|\alpha| \to 1$ and propose a cosmological solution that is consistent with observations.

The paper is organized as follows: in Section 2, we briefly review the fundamental equations of $f(R,T)$ gravity and derive the dynamical system. Section 3 shows phase diagrams on three invariant planes and obtains cosmological solutions. Section 4 contains the case $|\alpha| \to 1$ in 3D. Section 5 briefly analyzes a case that is considered to be more interesting and physical when $f(R,T) = R + \xi R^{\alpha} + \zeta\sqrt{-T}$. In Section 6, we summarize and discuss the obtained results.

2. Cosmological Equation in $f(R,T)$ Gravity

The action for the $f(R,T)$ gravity can be written as follows

$$S = \int \sqrt{-g} d^4x \left[\frac{1}{16\pi G} f\left(R, T^{(\mathrm{m})}\right) + L^{(\mathrm{m})} + L^{(\mathrm{rad})} \right], \tag{1}$$

where g is the determinant of the metric, $f(R,T)$ is an arbitrary function of the Ricci scalar R, and the trace of the energy-momentum tensor $T^{(\mathrm{m})}$, $L^{(\mathrm{m})}$, and $L^{(\mathrm{rad})}$ stand the Lagrangians of the dust matter and radiation, respectively, and we set c = 1. Since the trace of the radiation energy–momentum tensor $L^{(\mathrm{rad})}$ = 0, we drop the superscript m from the trace $T^{(\mathrm{m})}$. As usual, the energy-momentum tensor is defined as

$$T_{\mu\nu} \equiv -\frac{2}{\sqrt{-g}} \frac{\delta\left[\sqrt{-g}\left(L^{(\mathrm{m})} + L^{(\mathrm{rad})}\right)\right]}{\delta g^{\mu\nu}}, \tag{2}$$

Moreover, we assume that $L^{(\mathrm{m})}$ and $L^{(\mathrm{rad})}$ depend only on the metric and not on its derivatives. We obtain

$$T_{\mu\nu} = g_{\mu\nu}\left[L^{(\mathrm{m})} + L^{(\mathrm{rad})}\right] - 2\frac{\partial\left[L^{(\mathrm{m})} + L^{(\mathrm{rad})}\right]}{\partial g^{\mu\nu}}. \tag{3}$$

We assume a perfect fluid in the model and have

$$g^{\alpha\beta}\frac{\delta T^{(\mathrm{m})}}{\delta g^{\mu\nu}} = -2T^{(\mathrm{m})}_{\mu\nu}, \tag{4}$$

By varying the action S with respect to the $T_{\mu\nu}$, we obtain

$$\begin{aligned} f_R(R,T)R_{\mu\nu} - \frac{1}{2}f(R,T)g_{\mu\nu} + \left(g_{\mu\nu}\Box - \nabla_\mu\nabla_\nu\right)f_R(R,T) \\ = (8\pi G + f_T(R,T))T^{(\mathrm{m})}_{\mu\nu} + 8\pi G T^{(\mathrm{rad})}_{\mu\nu}, \end{aligned} \tag{5}$$

where $\Box = \nabla^\mu\nabla_\mu$, $f_R(R,T) = \partial f(R,T)/\partial R$, $f_T(R,T) = \partial f(R,T)/\partial T$ and ∇_μ denotes the covariant derivative. With the contraction of Equation (5), we have

$$f_R(R,T) + 3\Box f_R(R,T) - 2f(R,T) = (8\pi G + f_T(R,T))T. \tag{6}$$

Here, we consider a spatially flat FLRW metric given by

$$ds^2 = -dt^2 + a^2(t)\left(dx^2 + dy^2 + dz^2\right), \tag{7}$$

where $a(t)$ represents the scale factor. Equation (5) can be rewritten in a standard form

$$G_{\mu\nu} = \frac{8\pi G}{f_R(R,T)}\left(T^{(\mathrm{m})}_{\mu\nu} + T^{(\mathrm{rad})}_{\mu\nu} + T^{(\mathrm{eff})}_{\mu\nu}\right), \tag{8}$$

where

$$\begin{aligned} T^{(\mathrm{eff})}_{\mu\nu} =& \frac{1}{8\pi G}\left[\frac{1}{2}(f(R,T) - f_R(R,T)R)g_{\mu\nu} \right. \\ &+ \left. \left(\nabla_\mu\nabla_\nu - g_{\mu\nu}\Box\right)f_R(R,T) + f_T(R,T)T^{(\mathrm{m})}_{\mu\nu}\right]. \end{aligned} \tag{9}$$

According to the Bianchi identity, we can know that $\nabla^\mu T^{(\mathrm{m})}_{\mu\nu} = 0 = \nabla^\mu T(\mathrm{m})_{\mu\nu}$. Under the assumption of the conservation of the effective energy-momentum tensor $T^{(\mathrm{m})}_{\mu\nu}$, we find

$$\frac{3}{2}H(t)f_T(R,T) = \dot{f}_T(R,T), \tag{10}$$

where $H(t) = \dot{a}(t)/a(t)$ is the Hubble parameter, and a dot denotes the derivative with respect to the cosmic time t. Regarding the metric (7), Equations (5) and (6) can be given as

$$\begin{aligned} 3H^2 f_R(R,T) + \frac{1}{2}(f(R,T) - f_R(R,T)R) + 3\dot{f}_R(R,T)H \\ = (8\pi G + f_T(R,T))\rho^{(\mathrm{m})} + 8\pi G\rho^{(\mathrm{m})} \end{aligned} \tag{11}$$

and

$$2f_R(R,T)\dot{H} + \ddot{f}_R(R,T) - \dot{f}_R(R,T)H = -(8\pi G + f_T(R,T))\rho^{(\mathrm{m})} - \frac{32}{3}\pi G\rho^{(\mathrm{rad})}. \tag{12}$$

In the following, we assume that $f(R,T) = g(R) + h(T)$, where both $g(R)$ and $h(T)$, cannot be a constant. Six dimensionless independent variables are introduced to obtain the equations of dynamics [41], namely,

$$x_1 \equiv -\frac{\dot{g}'(R)}{Hg'(R)}, x_2 \equiv -\frac{g(R)}{6H^2 g'(R)}, x_3 \equiv \frac{R}{6H^2} = \frac{\dot{H}}{H^2} + 2, \tag{13}$$

$$x_4 \equiv -\frac{h(T)}{3H^2 g'(R)}, x_5 \equiv -\frac{8\pi G\rho^{(\mathrm{rad})}}{3H^2 g'(R)}, x_6 \equiv -\frac{Th'(T)}{3H^2 g'(R)}. \tag{14}$$

Four dimensionless parameters are defined for parameterization in the determination of the dynamic equations. These parameters are:

$$m \equiv \frac{Rg''(R)}{g'(R)}, r \equiv -\frac{Rg'(R)}{g(R)} = \frac{x_3}{x_2}, n \equiv \frac{Th''(T)}{h'(T)}, s \equiv \frac{Th'(T)}{h(T)} = \frac{x_6}{x_4}. \tag{15}$$

With the form $f(R,T) = g(R) + h(T)$, we rewrite Equations (11) and (12) as follows:

$$1 + \frac{g}{6H^2 g'} + \frac{h}{6H^2 g'} - \frac{R}{6H^2} + \frac{\dot{g}'}{Hg'} = \frac{8\pi G\rho^{(\mathrm{m})}}{3H^2 g'} + \frac{h'\rho^{(\mathrm{m})}}{3H^2 g'} + \frac{8\pi G\rho^{(\mathrm{rad})}}{3H^2 g'} \tag{16}$$

and

$$2\frac{\dot{H}}{H^2} + \frac{\ddot{g}'}{H^2 g'} - \frac{\dot{g}'}{Hg'} = -\frac{8\pi G\rho^{(\mathrm{m})}}{H^2 g'} - \frac{h'\rho^{(\mathrm{m})}}{H^2 g'} - \frac{32\pi G\rho^{(\mathrm{rad})}}{3H^2 g'}. \tag{17}$$

The constraint Equation (10) becomes

$$Th'' = -\frac{1}{2}h', \tag{18}$$

and by integrating with respect to the trace h, Equation (18) reads

$$Th' - \frac{1}{2}h + C = 0, \tag{19}$$

where C is an integration constant. Set $C = 0$, which leads to $s = 1/2$. Then, we obtain $x_4 = 2x_6$ and $h = \zeta\sqrt{-T}$, where ζ is a constant.

We consider the model's later-time behaviors, i.e., radiation does not exist, and assume that $f(R,T) = \xi R^{\alpha} + \zeta\sqrt{-T}$, where ξ is a constant. Thus, we obtain that

$$x_3 = -\alpha x_2, m = \alpha - 1. \tag{20}$$

By setting $x_1 \equiv x, x_2 \equiv y, x_4 \equiv z$, the obtained autonomous dynamical system is:

$$\begin{aligned} \frac{dx}{dN} &= -1 + x(x + \alpha y) + (\alpha - 3)y - \frac{3}{2}z, \\ \frac{dy}{dN} &= -\frac{xy}{\alpha - 1} + 2y(2 + \alpha y), \\ \frac{dz}{dN} &= z\left(\frac{5}{2} + x + 2\alpha y\right), \end{aligned} \tag{21}$$

where $N = \ln a$. We defined the density parameter of matter $\Omega^{(\mathrm{m})}$ and effective equation of state $\omega^{(\mathrm{eff})}$ as follows

$$\Omega^{(\mathrm{m})} \equiv \frac{8\pi G\rho^{(\mathrm{m})}}{3H^2 g'} = 1 - x + (\alpha - 1)y - z, \tag{22}$$

$$\omega^{(\mathrm{eff})} \equiv -1 - \frac{2\dot{H}}{3H^2} = \frac{1}{3}(1 + 2\alpha y). \tag{23}$$

System (21) has six finite equilibrium points p_i $(i = 1, \cdots, 6)$. Here, $p_1 = (1, 0, 0)$ has eigenvalues $2, 7/2$ and $(4\alpha - 5)/(\alpha - 1)$, $p_2 = (-1, 0, 0)$ has eigenvalues $-2, 3/2$, and $(4\alpha - 3)/(\alpha - 1)$, $p_3 = (-5/2, 0, 7/2)$ has eigenvalues $-7/2$, $-3/2$, and $(8\alpha - 3)/(\alpha - 1)$, $p_4 = ((4 - 2\alpha)/(2\alpha - 1), (5 - 4\alpha)/[(2\alpha - 1)(\alpha - 1)], 0)$ has eigenvalues $(5 - 4\alpha)/(\alpha - 1)$, $(-8\alpha^2 + 13\alpha - 3)/[(2\alpha - 1)(\alpha - 1)]$ and $-[(5\alpha - 1)(2\alpha - 3)]/[2(2\alpha - 1)(\alpha - 1)]$, $p_5 = ((5 - 4\alpha)/\alpha, (3 - 4\alpha/2\alpha^2, 0)$ has eigenvalues $3/2$ and

$$\left[3(1-\alpha) \pm \sqrt{(\alpha-1)(256\alpha^3 - 608\alpha^2 + 417\alpha - 81)}\right] / [4\alpha(\alpha - 1)],$$

and $p_6 = (3(\alpha - 1)/(2\alpha), (3 - 8\alpha)/(4\alpha^2), -[(5\alpha - 1)(2\alpha - 3)]/[4\alpha^2])$ has eigenvalues $-3/2$ and

$$\left[3(2\alpha-1)(\alpha-1) \pm \sqrt{(\alpha-1)(676\alpha^3 - 1328\alpha^2 + 573\alpha - 81)}\right] / [8\alpha(\alpha - 1)].$$

These equilibrium points of system (21) are presented in Table 1. According to different values of α, we summarize the relevant types of these six finite equilibrium points in Table 2.

Table 1. Equilibrium points of system (21).

Equilibrium Points	Coordinates (x, y, z)	Scale Factor	$\Omega^{(\mathrm{m})}$	$\omega^{(\mathrm{eff})}$
p_1	$(1, 0, 0)$	$a(t) = a_0\left(\frac{t-t_i}{t_0-t_i}\right)^{\frac{1}{2}}$	0	$\frac{1}{3}$
p_2	$(-1, 0, 0)$	$a(t) = a_0\left(\frac{t-t_i}{t_0-t_i}\right)^{\frac{1}{2}}$	2	$\frac{1}{3}$
p_3	$(-\frac{5}{2}, 0, \frac{7}{2})$	$a(t) = a_0\left(\frac{t-t_i}{t_0-t_i}\right)^{\frac{1}{2}}$	0	$\frac{1}{3}$
p_4	$(\frac{4-2\alpha}{2\alpha-1}, \frac{5-4\alpha}{(\alpha-1)(2\alpha-1)}, 0)$	$a(t) = a_0\left(\frac{t-t_i}{t_0-t_i}\right)^{\frac{(\alpha-1)(2\alpha-1)}{2-\alpha}}$	0	$\frac{-6\alpha^2+7\alpha+1}{3(\alpha-1)(2\alpha-1)}$
p_5	$(\frac{3(\alpha-1)}{\alpha}, \frac{3-4\alpha}{2\alpha^2}, 0)$	$a(t) = a_0\left(\frac{t-t_i}{t_0-t_i}\right)^{\frac{2\alpha}{3}}$	$\frac{-8\alpha^2+13\alpha-3}{2\alpha^2}$	$\frac{1-\alpha}{\alpha}$
p_6	$(\frac{3(\alpha-1)}{2\alpha}, \frac{3-8\alpha}{4\alpha^2}, \frac{-10\alpha^2+17\alpha-3}{4\alpha^2})$	$a(t) = a_0\left(\frac{t-t_i}{t_0-t_i}\right)^{\frac{4\alpha}{3}}$	0	$\frac{1-2\alpha}{2\alpha}$

Table 2. Finite equilibrium points and their types for different values of α of system (21).

Values of α	Finite Equilibrium Points
$\alpha < 0$ or $0 < \alpha < \frac{1}{5}$ or $\alpha > \frac{3}{2}$	p_1 is an unstable node, p_2, p_3, p_5 and p_6 are saddles, p_4 is a stable node
$\alpha = \frac{1}{5}$ or $\alpha = \frac{3}{2}$	p_1 is an unstable node, p_2, p_3, and p_5 are saddles, p_4 and p_6 have a 2DSM
$\frac{1}{5} < \alpha < \frac{13-\sqrt{73}}{16}$ or $\frac{13-\sqrt{73}}{16} < \alpha \leq \alpha_1$ or $\alpha_4 \leq \alpha < \frac{3}{2}$	p_1 is an unstable node, p_2, p_3, p_4 and p_5 are saddles, p_6 is a stable node
$\alpha = \frac{13-\sqrt{73}}{16}$	p_1 is an unstable node, p_2 and p_3 are saddles, p_4 and p_5 have a 1DUM and a 1DSM, p_6 is a stable node
$\alpha_1 < \alpha < \frac{3}{8}$	p_1 is an unstable node, p_2, p_3 and p_4 are saddles, p_5 is a NHEP, p_6 is a stable node
$\alpha = \frac{3}{8}$	p_1 is an unstable node, p_2 and p_4 are saddles, p_3 and p_6 have a 2DSM, p_5 is a NHEP
$\frac{3}{8} < \alpha < \frac{1}{2}$	p_1 is an unstable node, p_2, p_4 and p_6 are saddles, p_3 is a stable node, p_5 is a NHEP

Table 2. *Cont.*

Values of α	Finite Equilibrium Points
$\frac{1}{2} < \alpha < \alpha_2$	p_1 is an unstable node, p_2 and p_6 are saddles, p_3 and p_4 are stable nodes, p_5 is a NHEP
$\alpha_2 \leq \alpha < \frac{3}{4}$ or $\frac{3}{4} < \alpha < 1$	p_1 is an unstable node, p_2, p_5, and p_6 are saddles, p_3 and p_4 are stable nodes
$\alpha = \frac{3}{4}$	p_1 is an unstable node, p_2 and p_5 have a 1DUM and a 1DSM, p_3 and p_4 are stable nodes, p_6 is a saddle
$1 < \alpha < \frac{5}{4}$	p_1, p_2, and p_3 is a saddle, p_4 is an unstable node, p_5 and p_6 are NHEPs
$\alpha = \frac{5}{4}$	p_1 and p_4 have a 2DUM, p_2 and p_3 are saddles, p_5 and p_6 are NHEPs
$\frac{5}{4} < \alpha < \alpha_3$	p_1 is an unstable node, p_2, p_3, and p_4 are saddles, p_5 and p_6 are NHEPs
$\alpha_3 \leq \alpha < \frac{13+\sqrt{73}}{16}$ or $\frac{13+\sqrt{73}}{16} < \alpha < \alpha_4$	p_1 is an unstable node, p_2, p_3, p_4, and p_5 are saddles, p_6 is a NHEP
$\alpha = \frac{13+\sqrt{73}}{16}$	p_1 is an unstable node, p_2 and p_3 are saddles, p_4 and p_5 have a 1DUM and a 1DSM, p_6 is a NHEP

Note: 2DSM: two-dimensional stable manifold. 1DUM: one-dimensional unstable manifold. 1DSM: one-dimensional stable manifold. NHEP: non-hyperbolic equilibrium point.

3. Phase Portraits on Invariant Planes and Cosmological Solutions

For the careful analysis of the global phase portraits and the local phase portraits at the equilibrium points of system (21), we start our discussion on three invariant planes $z = 0$, $y = 0$, and $1 - x + (\alpha - 1)y - z = 0$, respectively. Note that the first two invariant planes are obvious, here we just need to verify that $1 - x + (\alpha - 1)y - z = 0$ is also an invariant plane of system (21). As $\Omega^{(\mathrm{m})} = 1 - x(\alpha - 1)y - z$, the surface $1 - x + (\alpha - 1)y - z = 0$ is invariant if it holds that

$$\frac{\partial \Omega^{(\mathrm{m})}}{\partial x} x' + \frac{\partial \Omega^{(\mathrm{m})}}{\partial y} y' + \frac{\partial \Omega^{(\mathrm{m})}}{\partial z} = K \Omega^{(\mathrm{m})}, \tag{24}$$

where K is a polynomial, and this is the case with $K = 1 + x + 2\alpha y$.

3.1. Phase Portraits on the Invariant Plane $z = 0$ and Cosmological Solutions

On this invariant plane, system (21) becomes

$$\begin{aligned} \frac{dx}{dN} &= -1 + x(x + \alpha y) + (\alpha - 3)y \\ \frac{dy}{dN} &= -\frac{xy}{\alpha - 1} + 2y(2 + \alpha y) \end{aligned} \tag{25}$$

System (25) has four finite equilibrium points $e_1 = (1, 0)$, $e_2 = (-1, 0)$, $e_4 = ((4 - 2\alpha)/(2\alpha - 1), (5 - 4\alpha)/[(\alpha - 1)(2\alpha - 1)])$ and $e_5 = (3(\alpha - 1)/\alpha, (3 - 4\alpha)/(2\alpha^2))$. In fact, the points e_i and the previous p_i $(i = 1, 2, 3, 4, 5, 6)$ represent the same location in space. Since the stability of the same location in 3D space and invariant planes may not be the same, the two forms p_i and e_i are used to distinction. We use p_i when discussing the stability of points in 3D space and e_i on an invariant plane.

The point e_1 is a purely kinetic point with $\Omega^{(\mathrm{m})} = 0$ and $\omega^{(\mathrm{eff})} = 1/3$. Since this point can not describe any known matter, it is not considered to have physical significance. The eigenvalues of e_1 are 2 and $(4\alpha - 5)/(\alpha - 1)$, it is an unstable node when $\alpha < 0$ or $0 < \alpha < 1$ or $\alpha > 5/4$, a saddle when $1 < \alpha < 5/4$ and a saddle-node when $\alpha = 5/4$.

The point e_2 is denoted as a ϕ-matter-dominated epoch (ϕMDE) [51] with $\Omega^{(\mathrm{m})} = 2$ and $\omega^{(\mathrm{eff})} = 1/3$. Although the matter-density parameter of e_2 does not match the effective equation of state, the universe may approach to this point in this model. The point e_2 can be treated as a special case of point e_5 by setting $\alpha = 3/4$. The point has eigenvalues -2 and $(4\alpha - 3)/(\alpha - 1)$, it is a saddle when $\alpha < 0$ or $0 < \alpha < 3/4$ or $\alpha > 1$, a stable node when $3/4 < \alpha < 1$ and a saddle-node when $\alpha = 3/4$.

For point e_4, we have $\Omega^{(\mathrm{m})} = 0$ and $\omega^{(\mathrm{eff})} = (-6\alpha^2 + 7\alpha + 1)/[3(\alpha - 1)(2\alpha - 1)]$. This point can act as an accelerated-expansion point provided that $\omega^{(\mathrm{eff})} < -1/3$ for $\alpha < (1 - \sqrt{3})/2$ or $\alpha > (1 + \sqrt{3})/2$ or $1/2 < \alpha < 1$. This point has eigenvalues $(5 - 4\alpha)/(\alpha - 1)$ and $(-8\alpha^2 + 13\alpha - 3)/[(\alpha - 1)(2\alpha - 1)]$, it is a stable node when $\alpha < 0$ or $0 < \alpha < \left(13 - \sqrt{73}\right)/16$ or $1/2 < \alpha < 1$ or $\alpha > \left(13 + \sqrt{73}\right)/16$, a saddle when $\left(13 - \sqrt{73}\right)/16 < \alpha < 1/2$ or $5/4 < \alpha < \left(13 + \sqrt{73}\right)/16$, an unstable node when $1 < \alpha < 5/4$ and a saddle-node when $\alpha = \left(13 \pm \sqrt{73}\right)/16$ or $5/4$. Thus, e_4 contains the range where the universe can be accelerated, i.e., $\alpha < (1 - \sqrt{3}/2)$ or $1/2 < \alpha < 1$ or $\alpha > (13 + \sqrt{73})/16$. Additionally, the point e_4 does not exist when $\alpha = 1/2$.

For point e_5, we have $\Omega^{(\mathrm{m})} = (-8\alpha^2 + 13\alpha - 3)/(2\alpha^2)$ and $\omega^{(\mathrm{eff})} = (1 - \alpha)/\alpha$. This point can actually represent a standard matter era with $\Omega^{(\mathrm{m})} = 1$ and $a \propto t^{2/3}$ when $\alpha \to 1$. However, when $\alpha < 0$ or $\alpha > 3/2$, e_5 can be the point of acceleration, but with a negative value for the matter-density parameter. Considering Equation (22), solutions that lead to $\Omega^{(\mathrm{m})} < 0$ are excluded from the background of feasible $f(R)$ models, so we discard it from the acceleration point candidates. The point e_5 has eigenvalues $\left[3(\alpha - 1) \pm \sqrt{(\alpha - 1)(256\alpha^3 - 608\alpha^2 + 417\alpha - 81)}\right]/[4\alpha(\alpha - 1)]$, it is a saddle when $\alpha < 0$ or $0 < \alpha < \left(13 - \sqrt{73}\right)/16$ or $3/4 < \alpha < 1$ or $\alpha > \left(13 + \sqrt{73}\right)/16$, a stable node when $\left(13 - \sqrt{73}\right)/16 < \alpha \leq \alpha_1$ or $\alpha_2 \leq \alpha < 3/4$ or $\alpha_3 \leq \alpha < \left(13 + \sqrt{73}\right)/16$, a stable focus when $\alpha_1 < \alpha < \alpha_2$ or $1 < \alpha < \alpha_3$ and a saddle-node when $\alpha = \left(13 \pm \sqrt{73}\right)/16$ or $3/4$. The constants α_1, α_2 and α_3 are the roots of $256\alpha^3 - 608\alpha^2 + 417\alpha - 81 = 0$ and $\alpha_1 < \alpha_2 < \alpha_3$.

The verification of situation that e_1 is a saddle-node when $\alpha = 5/4$ is presented here. When $\alpha = 5/4$, we set $x = p - 1$ and system (25) becomes

$$\begin{aligned} \frac{dp}{dN} &= p^2 + \frac{5}{4}py - 2p - 3y, \\ \frac{dy}{dN} &= -4py + \frac{5}{2}y^2 + 8y. \end{aligned} \tag{26}$$

It is quite clear that $e_1' = (0,0)$ is the equilibrium point of system (26). By setting $-4py + \frac{5}{2}y^2 + 8y = 0$, we can obtain

$$y = \frac{8}{5}p - \frac{16}{5}. \tag{27}$$

Let $D = p^2 + \frac{5}{4}py - 2p - 3y$ and connecting with Equation (27), we obtain

$$D = 3p^2 - \frac{54}{5}p + \frac{48}{5}. \tag{28}$$

According to the semi-hyperbolic singular point theorem in [52], e_1' is a saddle-node. Thus, e_1 is also a saddle-node. Similar judgments will not be repeated below.

In order to investigate the infinite situation of system (25), we use the Poincaré compactification [52]. On the local chart U_1, set $x = 1/v$, $y = u/v$, then system (25) can be rewritten as

$$\begin{aligned}\frac{du}{dN} &= u\left[(3-\alpha)uv + v^2 + \alpha u + 4v - \frac{\alpha}{\alpha-1}\right],\\ \frac{dv}{dN} &= v\left[(3-\alpha)uv + v^2 - \alpha u - 1\right].\end{aligned} \tag{29}$$

Note that the time scale here is different from the previous N, but we still use the N notation for convenience.

At infinity $v = 0$ system (29) has two equilibrium points $e_7 = (0,0)$, $e_8 = (1/(\alpha-1), 0)$. The equilibrium point e_7 has eigenvalues -1 and $\alpha/(1-\alpha)$, it is a stable node when $\alpha < 0$ or $\alpha > 1$ and a saddle when $0 < \alpha < 1$. The equilibrium point e_8 has eigenvalues $\alpha/(\alpha-1)$, $(2\alpha-1)/(1-\alpha)$, it is a saddle when $\alpha < 0$ or $1/2 < \alpha < 1$ or $\alpha > 1$, a stable node when $0 < \alpha < 1/2$ and a saddle-node when $\alpha = 1/2$.

Similar to the local chart U_1 we let $x = u/v$, $y = 1/v$ on the local chart U_2, then system (25) has the form

$$\begin{aligned}\frac{du}{dN} &= \frac{\alpha}{\alpha-1}u^2 - v^2 - 4uv - \alpha u - (\alpha-3)v,\\ \frac{dv}{dN} &= v\left(\frac{1}{\alpha-1}u - 4v - 2\alpha\right).\end{aligned} \tag{30}$$

As other equilibrium points at infinity have been analyzed on the U_1, we only have to analyze the origin of system (30) on local chart U_2. Obviously the origin $e_9 = (0,0)$ is an equilibrium point of system (30). The equilibrium point e_9 has eigenvalues $-\alpha$ and -2α, it is an unstable node when $\alpha < 0$ and a stable node when $0 < \alpha < 1$ or $\alpha > 1$. The infinite points e_7, e_8, and e_9 are neither matter points nor feasible accelerated points because their matter-density parameters are negative.

Since the above four finite equilibrium points and three infinite equilibrium points have different stabilities when α varies, we make a summary in Table 3. Moreover, we present the global phase portraits of system (21) on the $z = 0$ in Figure 1, where the point $e_{i,j}$ can represent either e_i or e_j.

Here, we focus on the cosmological solutions that have survived a sufficiently long epoch of matter dominance, followed by accelerated expansion. In the phase space, we need to search for saddle points with positive matter-density parameters and stable points that can exhibit accelerated expansion. The points involving matter points are e_2 and e_5, and only e_4 can be the accelerated point on the invariant plane $z = 0$ in the model. Since the matter density parameter of e_2 exceeds the critical density of 1, we do not consider it as a matter point. The point e_5 is a saddle matter point when $1/2 < \alpha < 1$ and when $\alpha < (1-\sqrt{3})/2$ or $1/2 < \alpha < 1$ or $\alpha > (1+\sqrt{3})/2$, e_4 can be a stable accelerated point. For the limit $|\alpha| \to 0$ and 1, it can be found that under the limit $|\alpha| \to 0$, the point e_4 is not an accelerated point. When $\alpha \to 1^+$, the point e_4 is not an accelerated point, thus the trajectory from e_5 to e_4 is not a cosmological solution. The point e_5 is the saddle matter point and e_4 is a stable accelerated point when $\alpha \to 1^-$. Therefore, the trajectory from e_5 to e_4 can be a cosmological solution. The process from e_5 to e_4 can be regarded as a cosmological solution when $1/2 < \alpha < 3/4$, but there is no trajectory from e_5 to e_4 in this range. Therefore, the trajectory from e_5 to e_4 can be a cosmological solution when $3/4 \leq \alpha < 1$, however $m_5 = Rg''(R)/g'(R) < 0$ represents the divergence of the eigenvalues as $m_5 \to 1^-$. This means that the system can not remain around the point e_5 for a long time. Thus, there are no viable cosmological solutions on the invariant plane $z = 0$.

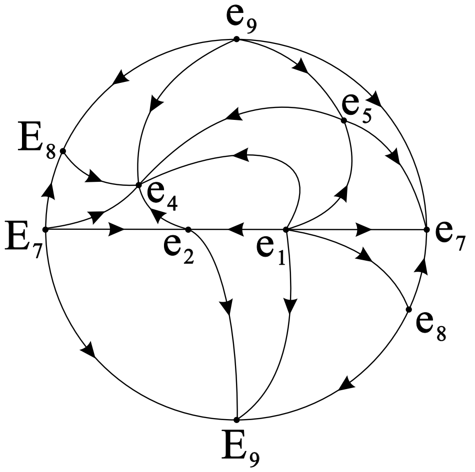

(**a**) $\alpha < 0$

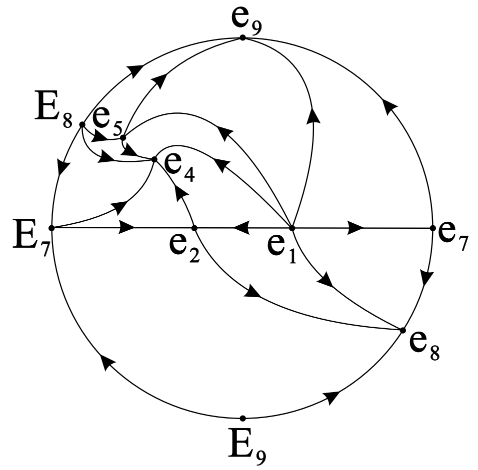

(**b**) $0 < \alpha < \frac{13-\sqrt{73}}{16}$

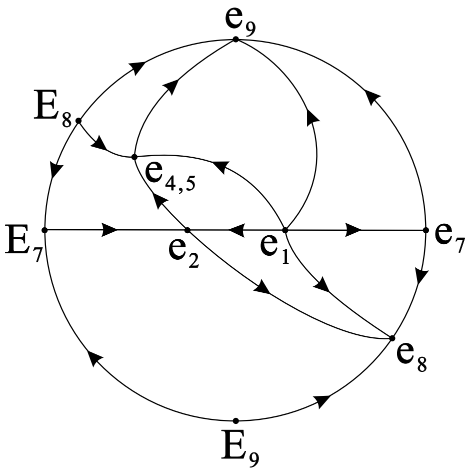

(**c**) $\alpha = \frac{13-\sqrt{73}}{16}$

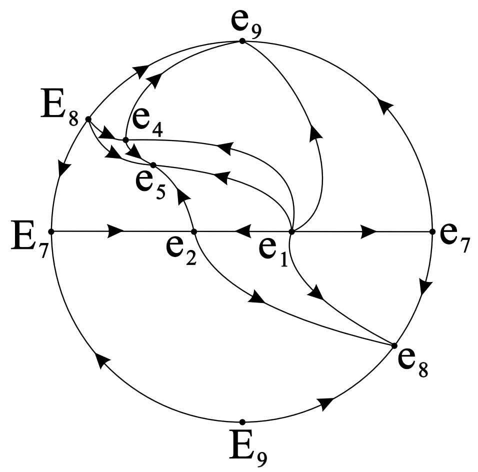

(**d**) $\frac{13-\sqrt{73}}{16} < \alpha \leq \alpha_1$

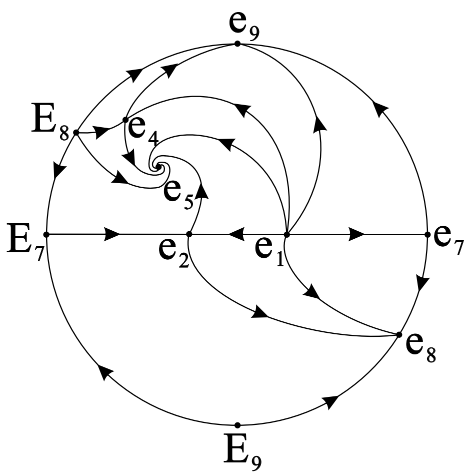

(**e**) $\alpha_1 < \alpha < \frac{1}{2}$

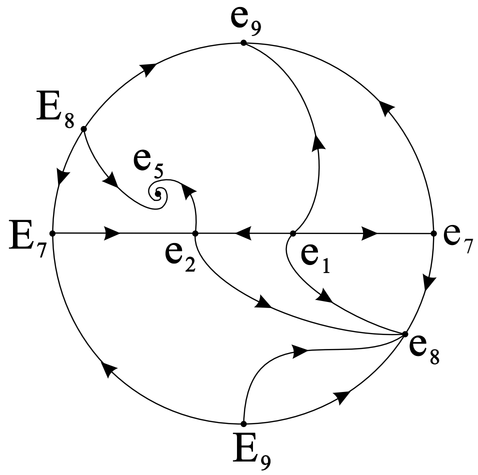

(**f**) $\alpha = \frac{1}{2}$

Figure 1. *Cont*.

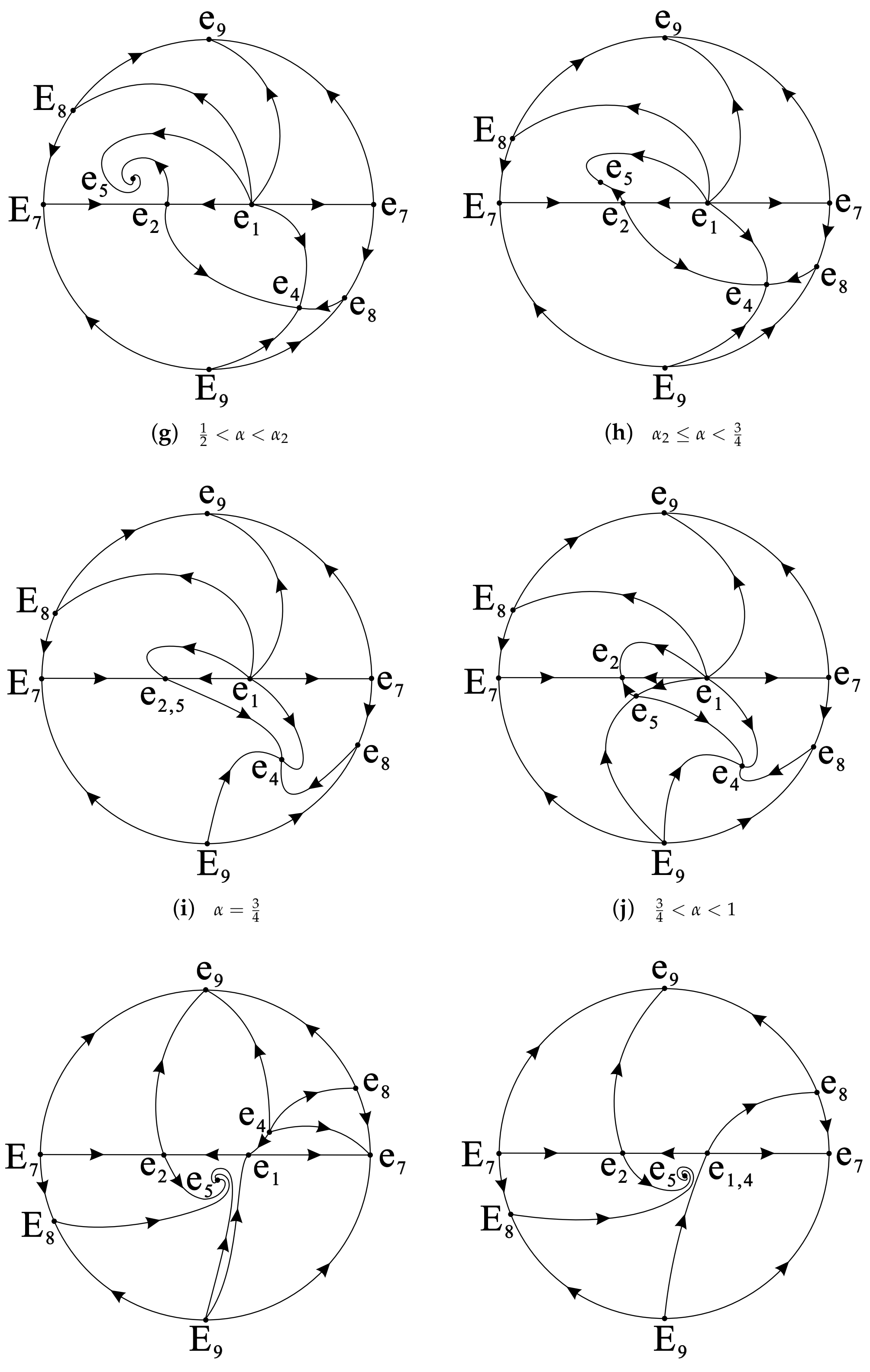

(**g**) $\frac{1}{2} < \alpha < \alpha_2$ (**h**) $\alpha_2 \leq \alpha < \frac{3}{4}$

(**i**) $\alpha = \frac{3}{4}$ (**j**) $\frac{3}{4} < \alpha < 1$

(**k**) $1 < \alpha < \frac{5}{4}$ (**l**) $\alpha = \frac{5}{4}$

Figure 1. *Cont.*

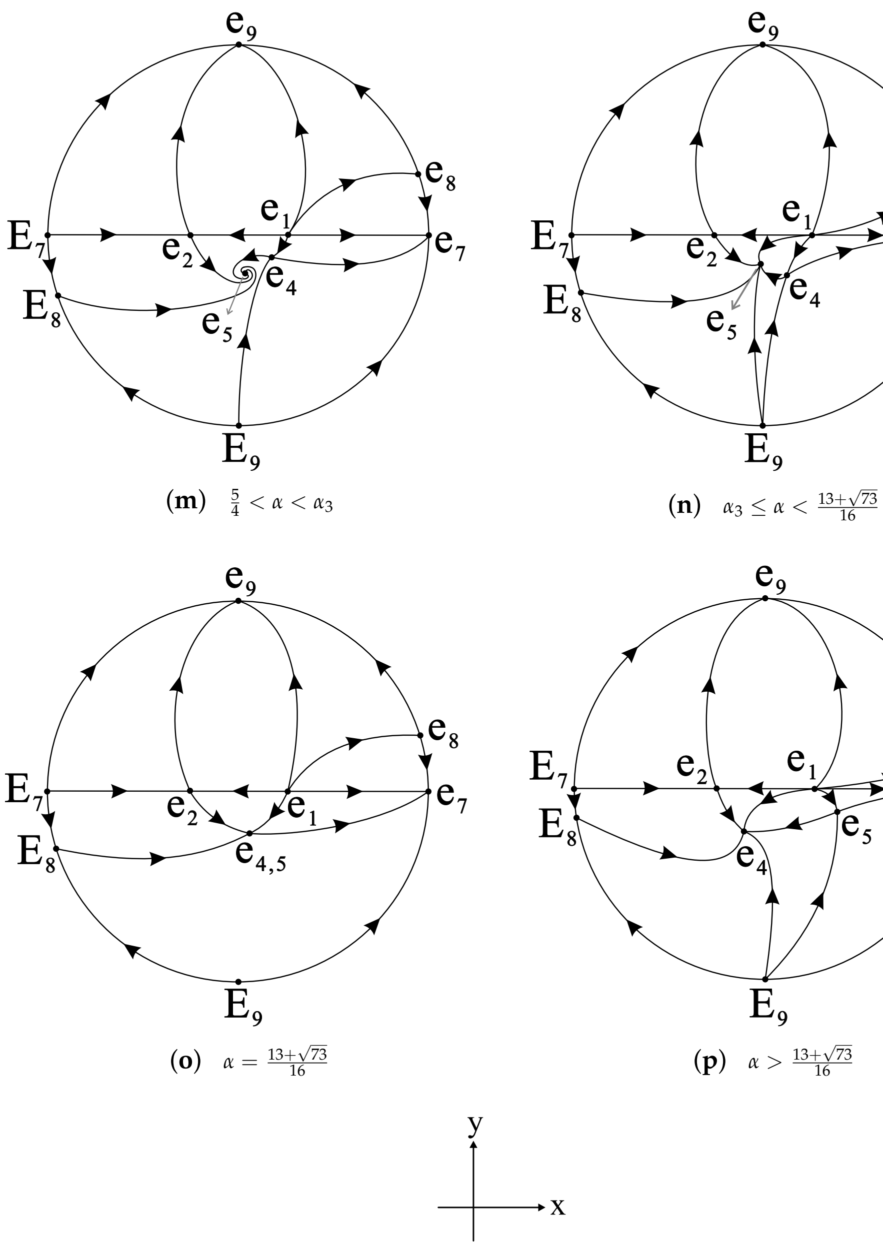

Figure 1. (**a**–**p**) Phase portraits on $z = 0$.

3.2. Phase Portraits on the Invariant Plane $y = 0$ and Cosmological Solutions

On the invariant plane $y = 0$ system (21) is

$$\begin{aligned} \frac{dx}{dN} &= -1 + x^2 - \frac{3}{2}z, \\ \frac{dy}{dN} &= z\left(x + \frac{5}{2}\right). \end{aligned} \tag{31}$$

System (31) has three equilibrium points, i.e., $e_1 = (1,0)$, $e_2 = (-1,0)$, and $e_3 = (-5/2, 7/2)$. Since the discussion of e_1 and e_2 has been presented above, we only discuss the point e_3 here. The point e_3 indicates $\Omega^{(m)} = 0$ and $\omega^{(\mathrm{eff})} = 1/3$. Since radiation is not present in the model, this point does match any known matter and is not physically interesting. The eigenvalues are $-3/2$ and $-7/2$, thus e_3 is a stable node.

Table 3. Equilibrium points and their types corresponding to various α values of system (25).

Values of α	Finite Equilibrium Points	Infinite Equilibrium Points
$\alpha < 0$	e_1 is an unstable node, e_2 and e_5 are saddles, e_4 is a stable node	e_7 is a stable node, e_8 is a saddle, e_9 is an unstable node
$0 < \alpha < \frac{13-\sqrt{73}}{16}$	e_1 is an unstable node, e_2 and e_5 are saddles, e_4 is a stable node	e_7 is a saddle, e_8 and e_9 are stable nodes
$\alpha = \frac{13-\sqrt{73}}{16}$	e_1 is an unstable node, e_2 is a saddle, e_4 and e_5 are saddle-nodes	e_7 is a saddle, e_8 and e_9 are stable nodes
$\frac{13-\sqrt{73}}{16} < \alpha \leq \alpha_1$	e_1 is an unstable node, e_2 and e_4 are saddles, e_5 is a stable node	e_7 is a saddle, e_8 and e_9 are stable nodes
$\alpha_1 < \alpha < \frac{1}{2}$	e_1 is an unstable node, e_2 and e_4 are saddles, e_5 is a stable focus	e_7 is a saddle, e_8 and e_9 are stable nodes
$\alpha = \frac{1}{2}$	e_1 is an unstable node, e_2 is a saddle, e_5 is a stable focus	e_7 is a saddle, $e_{4,8}$ is a saddle-node, e_9 is a stable node
$\frac{1}{2} < \alpha < \alpha_2$	e_1 is an unstable node, e_2 is a saddle, e_4 is a stable node, e_5 is a stable focus	e_7 and e_8 are saddles, e_9 is a stable node
$\alpha_2 \leq \alpha < \frac{3}{4}$	e_1 is an unstable node, e_2 is a saddle, e_4 and e_5 are stable nodes	e_7 and e_8 are saddles, e_9 is a stable node
$\alpha = \frac{3}{4}$	e_1 is an unstable node, e_2 and e_5 are saddle-nodes, e_4 is a stable node	e_7 and e_8 are saddles, e_9 is a stable node
$\frac{3}{4} < \alpha < 1$	e_1 is an unstable node, e_2 and e_4 are stable nodes, e_5 is a saddle	e_7 and e_8 are saddles, e_9 is a stable node
$1 < \alpha < \frac{5}{4}$	e_1 and e_2 are saddles, e_4 is an unstable node, e_5 is a stable focus	e_7 and e_9 are stable nodes, e_8 is a saddle
$\alpha = \frac{5}{4}$	e_1 and e_4 are saddle-nodes, e_2 is a saddle, e_5 is a stable focus	e_7 and e_9 are stable nodes, e_8 is a saddle
$\frac{5}{4} < \alpha < \alpha_3$	$e_1$is an unstable node, e_2 and e_4 are saddles, e_5 is a stable focus	e_7 and e_9 are stable nodes, e_8 is a saddle
$\alpha_3 \leq \alpha < \frac{13+\sqrt{73}}{16}$	$e_1$is an unstable node, e_2 and e_4 are saddles, e_5 is a stable node	e_7 and e_9 are stable nodes, e_8 is a saddle
$\alpha = \frac{13+\sqrt{73}}{16}$	$e_1$is an unstable node, e_2 is a saddle, e_4 and e_5 are saddle-nodes	e_7 and e_9 are stable nodes, e_8 is a saddle
$\alpha > \frac{13+\sqrt{73}}{16}$	e_1 is an unstable node, e_2 and e_5 are saddles, e_4 is a stable node	e_7 and e_9 are stable nodes, e_8 is a saddle

With the use of Poincaré compactification, we set $x = 1/v$, $z = u/v$ on the local chart U_1. System (31) reads

$$\begin{aligned}\frac{du}{dN} &= uv\left(\frac{3}{2}u + v + \frac{5}{2}\right),\\ \frac{dv}{dN} &= v\left(\frac{3}{2}uv + v^2 - 1\right).\end{aligned} \tag{32}$$

As all the points of system (32) at infinity $v = 0$ are equilibrium points, using the transformation $d\tau_1 = vdN$, we rewrite this system

$$\begin{aligned}\frac{du}{d\tau_1} &= u\left(\frac{3}{2}u + v + \frac{5}{2}\right),\\ \frac{dv}{d\tau_1} &= \frac{3}{2}uv + v^2 - 1.\end{aligned} \tag{33}$$

However, none of the points at $v = 0$ is the equilibrium point of system (33).

Similarly, we let $x = u/v$ and $z = 1/v$ on the local chart U_2. Then, system (31) is

$$\begin{aligned} \frac{du}{dN} &= -v\left(\frac{5}{2}u + v + \frac{3}{2}\right), \\ \frac{dv}{dN} &= -v\left(u - \frac{5}{2}v\right). \end{aligned} \tag{34}$$

The origin $e_{10} = (0, 0)$ is an equilibrium point of system (34). Although it has eigenvalues 0 and $3/2$, e_{10} is not a semi-hyperbolic point as it is not an isolated singular point of system (34). Note that all the points on the axis $v = 0$ are the equilibria of system (34) and there are no other equilibria on the axis $v = 0$ if we remove the common factor v. In the region near e_{10}, $5u/2 + v + 3/2 > 0$, $du/dN < 0$ for the positive semi-axis (PSA) of v illustrates that u decreases monotonously and $du/dN > 0$ for the negative semi-axis (NSA) of v indicates that u increases monotonously. Above the straight line $u + 5v/2 = 0$, $dv/dN < 0$ for the PSA of v and $du/dN > 0$ for the NSA of v. Below the straight line $u + 5v/2 = 0$, $dv/dN > 0$ for the PSA of v and $du/dN < 0$ for the NSA of v. Therefore, we obtain the local phase portrait of e_{10}, which is shown in Figure 2. Since the points at infinity have negative values of the matter-density parameter, they can not be an epoch of the universe.

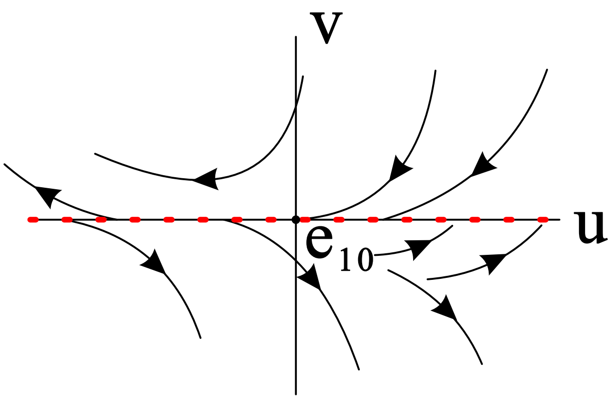

Figure 2. Local phase portrait of e_{10}.

We present the global phase portraits of system (31) on $y = 0$ in Figure 3. None of the points on the invariant plane $y = 0$ can show accelerated expansion, so we can not find a cosmological solution in Figure 3.

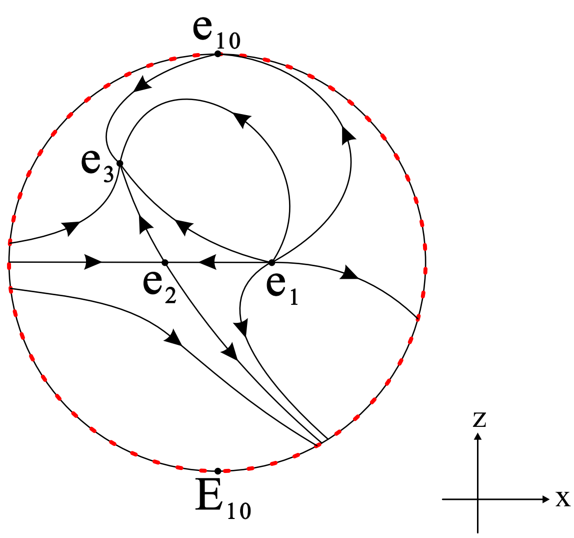

Figure 3. Phase portraits on $y = 0$.

3.3. *Phase Portraits on the Invariant Plane* $1-x+(\alpha-1)y-z=0$ *and Cosmological Solutions*

On this invariant plane system (21) changes to the form

$$\begin{aligned}\frac{dy}{dN}&=y\left[(2\alpha-1)y+\frac{1}{\alpha-1}z+\frac{4\alpha-5}{\alpha-1}\right],\\ \frac{dz}{dN}&=z\left[(3\alpha-1)y-z+\frac{7}{2}\right].\end{aligned} \tag{35}$$

System (35) has four equilibrium points $e_1=(0,0)$, $e_3=(0,7/2)$, $e_4=((5-4\alpha)/[(2\alpha-1)(\alpha-1)],0)$, and $e_6=((3-8\alpha)/(4\alpha^2),-[(2\alpha-3)(5\alpha-1)]/(4\alpha^2))$. According to the previous discussion, except for the point e_6, the physical meaning of other points is the same, but the mathematical stability may be different, so here we mainly discuss the point e_6. This point means $\Omega^{(\mathrm{m})}=0$ and $\omega^{(\mathrm{eff})}=(1-2\alpha)/(2\alpha)$. It can display an accelerated-expansion era for $\alpha<0$ or $\alpha>3/4$. The eigenvalues of e_6 are given by $-\left[3(\alpha-1)(2\alpha+1)\pm\sqrt{(\alpha-1)(676\alpha^3-1328\alpha^2+573\alpha-81)}\right]/[8\alpha(\alpha-1)]$, it is a saddle when $\alpha<0$ or $0<\alpha<1/5$ or $3/8<\alpha<1$ or $\alpha>3/2$, it is a stable node when $1/5<\alpha<3/8$ or $\alpha_4\le\alpha<3/2$, a stable focus when $1<\alpha<\alpha_4$ and a saddle-node when $\alpha=1/5,3/8,3/2$. The constant α_4 is the root of $676\alpha^3-1328\alpha^2+573\alpha-81=0$.

Applying the Poincaré compactification on the local chart U_1, we transform system (35) into

$$\begin{aligned}\frac{du}{dN}&=u\left[\frac{\alpha}{1-\alpha}u+\frac{3-\alpha}{2(\alpha-1)}+\alpha\right],\\ \frac{dv}{dN}&=v\left(\frac{1}{1-\alpha}u+\frac{4\alpha-5}{1-\alpha}v-2\alpha+1\right).\end{aligned} \tag{36}$$

At infinity $v=0$, system (36) has two equilibrium points, which are $e_{11}=(0,0)$ and $e_{12}=(\alpha-1,0)$. The equilibrium point e_{11} has eigenvalues α and $1-2\alpha$, it is a saddle when $\alpha<0$ or $1/2<\alpha<1$ or $\alpha>1$, an unstable node when $0<\alpha<1/2$ and a saddle-node when $\alpha=1/2$. The equilibrium point e_{12} has eigenvalues $-\alpha$ and -2α, it is an unstable node when $\alpha<0$ and a stable node when $0<\alpha<1$ or $\alpha>1$.

On the local chart U_2, we use the Poincaré compactification again changing system (35) to

$$\begin{aligned}\frac{du}{dN}&=u\left[-\alpha u+\frac{\alpha-3}{2(\alpha-1)}v+\frac{\alpha}{\alpha-1}\right],\\ \frac{dv}{dN}&=v\left[(1-3\alpha)u-\frac{7}{2}v+1\right].\end{aligned} \tag{37}$$

The equilibrium point $e_{13}=(0,0)$ is the origin of system (37). This point has eigenvalues 1 and $\alpha/(\alpha-1)$, it is an unstable node when $\alpha<0$ or $\alpha>1$ and a saddle when $0<\alpha<1$.

For points e_{11}, e_{12}, and e_{13} we all have $\Omega^{(\mathrm{m})}=0$. These points can be accelerated points when $\alpha<0$, however, they are not stable points in this range. Therefore, these three infinite points are not included in the cosmological solutions.

Since the stabilities of these four finite equilibrium points (e_1, e_3, e_4, and e_6) and three infinite equilibrium points (e_{11}, e_{12}, and e_{13}) are different when α changes, we make a summary in Table 4. Moreover, we present the global phase portraits of system (35) on $1-x+(\alpha-1)y-z=0$ in Figure 4. On the invariant plane $1-x+(\alpha-1)y-z=0$, the matter-density parameters are zero at all the equilibrium points. Since we can not find any matter points, there is no cosmological solution in Figure 4.

Table 4. Equilibrium points and their types for different values of α of system (35).

Values of α	**Finite Equilibrium Points**	**Infinite Equilibrium Points**
$\alpha < 0$	e_1 is an unstable node, e_3 and e_6 are saddles, e_4 is a stable node	e_{11} is a saddle, e_{12} and e_{13} are unstable nodes
$0 < \alpha < \frac{1}{5}$	e_1 is an unstable node, e_3 and e_6 are saddles, e_4 is a stable node	e_{11} is an unstable node, e_{12} is a stable node, e_{13} is a saddle
$\alpha = \frac{1}{5}$	e_1 is an unstable node, e_3 is a saddle, e_4 and e_6 are saddle-nodes	e_{11} is an unstable node, e_{12} is a stable node, e_{13} is a saddle
$\frac{1}{5} < \alpha < \frac{3}{8}$	e_1 is an unstable node, e_3 and e_4 are saddles, e_6 is a stable node	e_{11} is an unstable node, e_{12} is a stable node, e_{13} is a saddle
$\alpha = \frac{3}{8}$	e_1 is an unstable node, e_3 and e_6 are saddle-nodes, e_4 is a saddle	e_{11} is an unstable node, e_{12} is a stable node, e_{13} is a saddle
$\frac{3}{8} < \alpha < \frac{1}{2}$	e_1 is an unstable node, e_3 is a stable node, e_4 and e_6 are saddles	e_{11} is an unstable node, e_{12} is a stable node, e_{13} is a saddle
$\alpha = \frac{1}{2}$	e_1 is an unstable node, e_3 is a stable node, e_6 is a saddle	e_{11} is a saddle-node, e_{12} is a stable node, e_{13} is a saddle
$\frac{1}{2} < \alpha < 1$	e_1 is an unstable node, e_3 and e_4 are stable nodes, e_6 is a saddle	e_{11} and e_{13} are saddles, e_{12} is a stable node
$1 < \alpha < \frac{5}{4}$	e_1 and e_3 are saddles, e_4 is an unstable node, e_6 is a stable focus	e_{11} is a saddle, e_{12} is a stable node, e_{13} is an unstable node
$\alpha = \frac{5}{4}$	e_1 and e_4 are saddle-nodes, e_3 is a saddle, e_6 is a stable focus	e_{11} is a saddle, e_{12} is a stable node, e_{13} is an unstable node
$\frac{5}{4} < \alpha < \alpha_4$	e_1 is an unstable node, e_3 and e_4 are saddles, e_6 is a stable focus	e_{11} is a saddle, e_{12} is a stable node, e_{13} is an unstable node
$\alpha_4 \leq \alpha < \frac{3}{2}$	e_1 is an unstable node, e_3 and e_4 are saddles, e_6 is a stable node	e_{11} is a saddle, e_{12} is a stable node, e_{13} is an unstable node
$\alpha = \frac{3}{2}$	e_1 is an unstable node, e_3 is a saddle, e_4 and e_6 are saddle-nodes	e_{11} is a saddle, e_{12} is a stable node, e_{13} is an unstable node
$\alpha > \frac{3}{2}$	e_1 is an unstable node, e_3 and e_6 are saddles, e_4 is a stable node	e_{11} is a saddle, e_{12} is a stable node, e_{13} is an unstable node

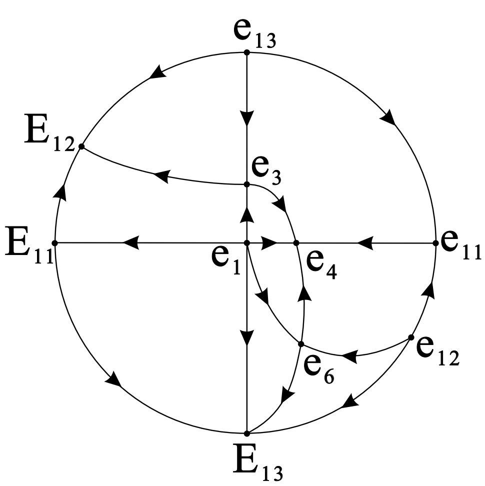

(a) $\alpha < 0$

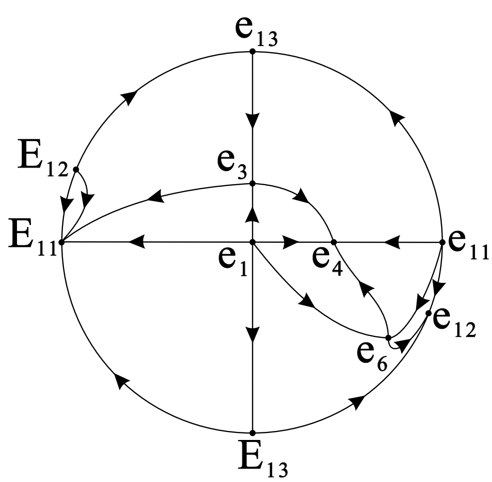

(b) $0 < \alpha < \frac{1}{5}$

Figure 4. *Cont.*

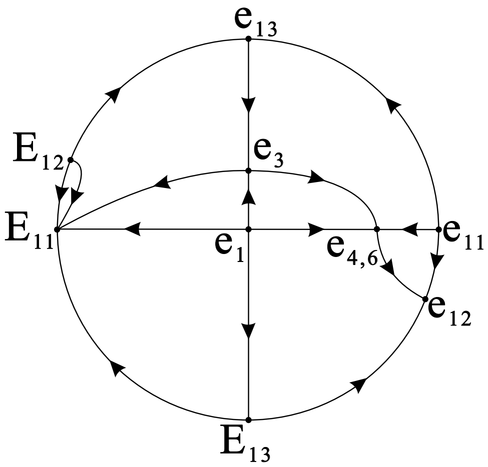

(c) $\alpha = \frac{1}{5}$

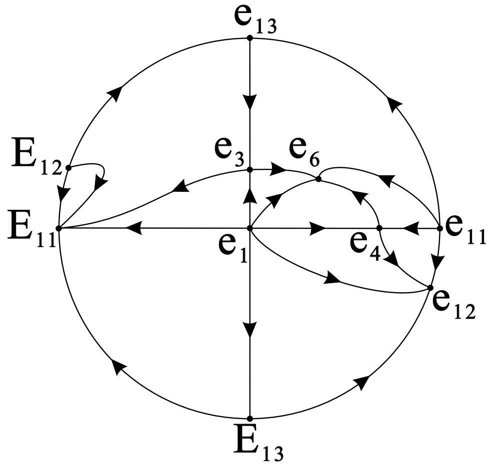

(d) $\frac{1}{5} < \alpha < \frac{3}{8}$

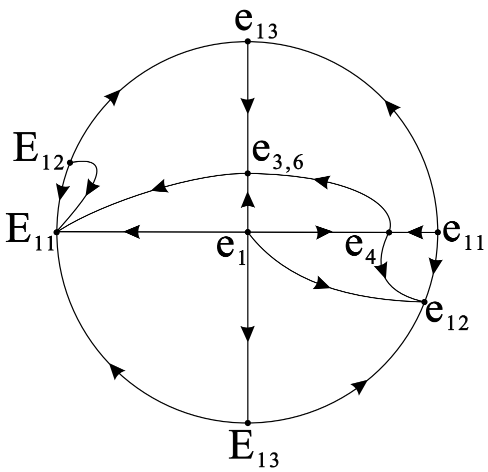

(e) $\alpha = \frac{3}{8}$

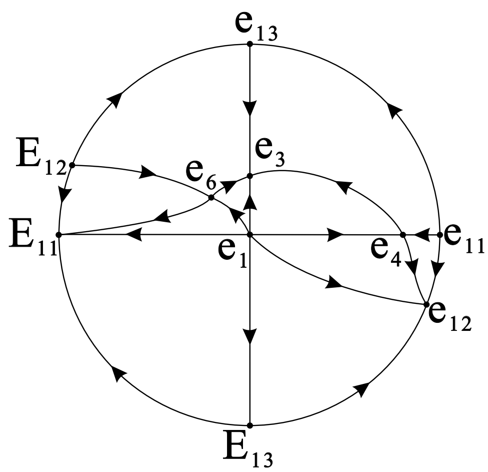

(f) $\frac{3}{8} < \alpha < \frac{1}{2}$

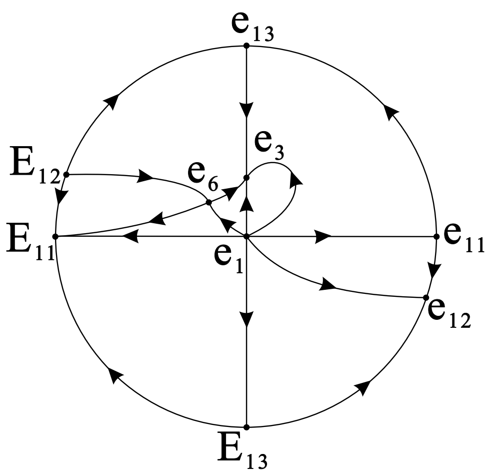

(g) $\alpha = \frac{1}{2}$

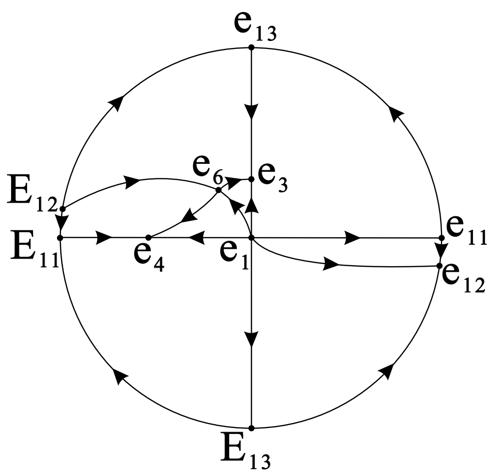

(h) $\frac{1}{2} < \alpha < 1$

Figure 4. *Cont*.

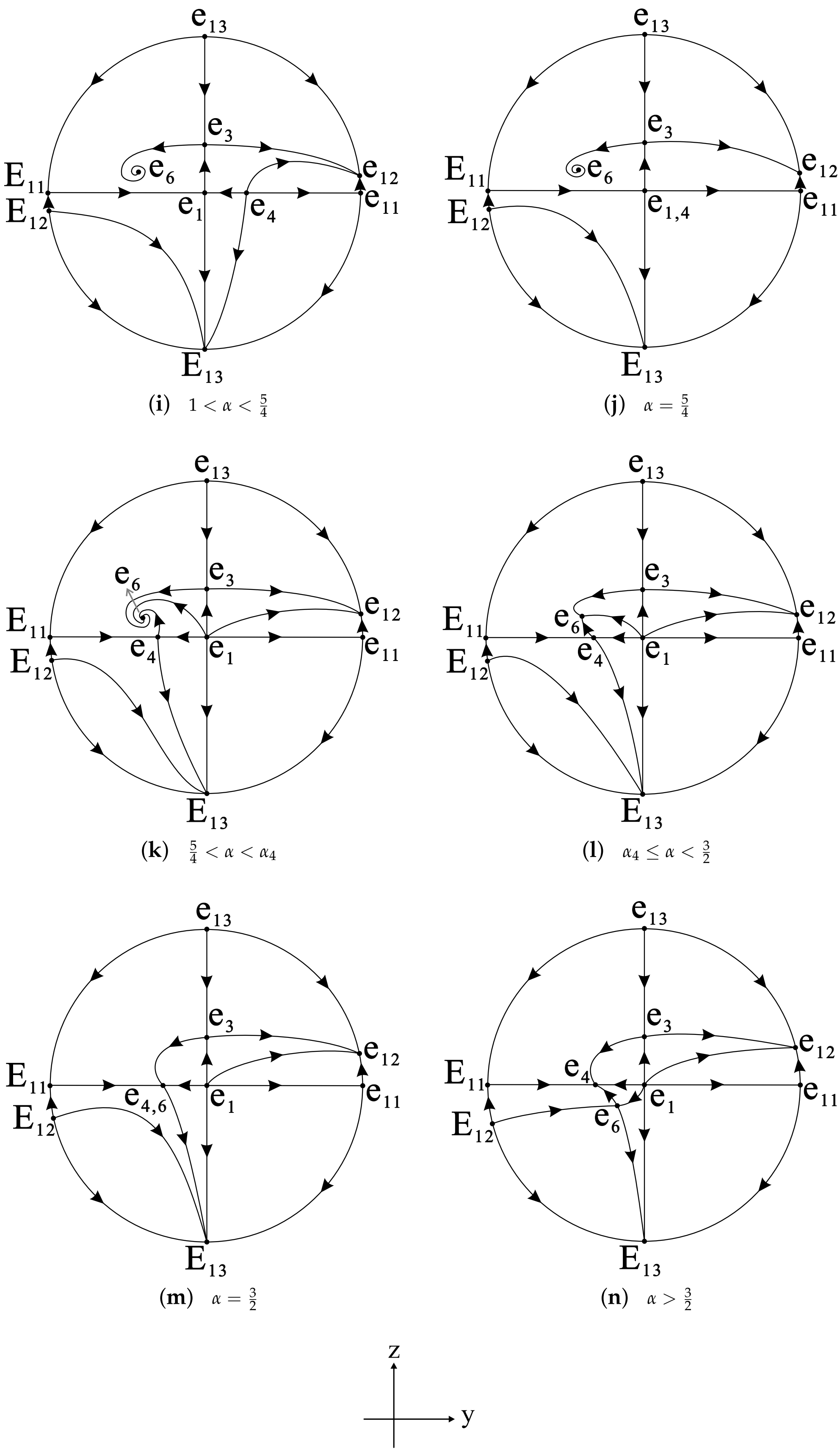

Figure 4. (**a**–**n**) Phase portraits on $1 - x + (\alpha - 1)y - z = 0$.

3.4. Equilibrium Points on the Poincaré Sphere at Infinity

Using the 3D Poincaré compactification [49,53], we let $x = 1/z_3$, $y = z_1/z_3$, $z = z_2/z_3$ on the local chart U_1 and then system (21) becomes

$$\begin{aligned}
\frac{dz_1}{dN} &= z_1\left[(3-\alpha)z_1z_3 + \frac{3}{2}z_2z_3 + z_3^2 + \alpha z_1 + 4z_3 - \frac{\alpha}{\alpha-1}\right],\\
\frac{dz_2}{dN} &= z_2\left[(3-\alpha)z_1z_3 + \frac{3}{2}z_2z_3 + z_3^2 + \alpha z_1 + \frac{5}{2}z_3\right],\\
\frac{dz_3}{dN} &= z_3\left[(3-\alpha)z_1z_3 + \frac{3}{2}z_2z_3 + z_3^2 - \alpha z_1 - 1\right].
\end{aligned} \tag{38}$$

As $z_3 = 0$ corresponds to the infinity, we only need to study equilibrium points with $z_3 = 0$ on the different local chart of Poincaré sphere. System (38) has equilibrium points $p_7 = (1/(\alpha-1), 0, 0)$ and $(0, z_2, 0)$ for all $z_2 \in \mathbb{R}$ when $z_3 = 0$. The equilibrium point P_7 has eigenvalues $(2\alpha-1)/(1-\alpha)$, $\alpha/(\alpha-1)$ and $\alpha/(\alpha-1)$, it is a stable node when $0 < \alpha < 1/2$ and it is a saddle when $\alpha < 0$ or $1/2 < \alpha < 1$ or $\alpha > 1$. The equilibrium point $(0, z_2, 0)$ has eigenvalues -1, 0, and $\alpha/(1-\alpha)$. Applying the normally hyperbolic sub-manifold theorem [54], the equilibrium point $(0, z_2, 0)$ has a two-dimensional stable manifold when $\alpha < 0$ or $\alpha > 1$ and when $0 < \alpha < 1$, it has a one-dimensional unstable manifold and a one-dimensional stable manifold.

Similar to the local chart U_1, we set $x = z_1/z_3$, $y = 1/z_3$, $z = z_2/z_3$ on U_2. we obtain

$$\begin{aligned}
\frac{dz_1}{dN} &= \frac{\alpha}{\alpha-1}z_1^2 - 4z_1z_3 - \frac{3}{2}z_2z_3 - z_3^2 - \alpha z_1 + (\alpha-3)z_3,\\
\frac{dz_2}{dN} &= z_2\left(\frac{\alpha}{\alpha-1}z_1 - \frac{3}{2}z_3\right),\\
\frac{dz_3}{dN} &= z_3\left(\frac{1}{\alpha-1}z_1 - 4z_3 - 2\alpha\right).
\end{aligned} \tag{39}$$

System (39) has an equilibrium point $p_9 = (\alpha-1, 0, 0)$ when $z_2 = 0$ and $z_3 = 0$. The equilibrium point p_9 has eigenvalues α, α, and $1-2\alpha$, it is an unstable node when $0 < \alpha < 1/2$ and it is a saddle when $\alpha < 0$ or $1/2 < \alpha < 1$ or $\alpha > 1$. Since other infinite equilibrium points of system (39) are contained in the local chart U_1, we will not analyze them.

Similarly, we have $x = z_1/z_3$, $y = z_2/z_3$, and $z = 1/z_3$ on the local chart U_3 and then system (21) is

$$\begin{aligned}
\frac{dz_1}{dN} &= -\alpha z_1z_2 - \frac{5}{2}z_1z_3 + (\alpha-3)z_2z_3 - z_3^2 - \frac{3}{2}z_3,\\
\frac{dz_2}{dN} &= z_2\left(\frac{\alpha}{1-\alpha}z_1 + \frac{3}{2}z_3\right),\\
\frac{dz_3}{dN} &= z_3\left(-z_1z_3 - 2\alpha z_2 - \frac{5}{2}z\right).
\end{aligned} \tag{40}$$

The origin $p_{10} = (0, 0, 0)$ of system (40) is an equilibrium point. In the local chart U_3, we will not study other equilibria of system (40) expect p_{10} because they have been discussed on the local charts U_1 and U_2. We take $z_3 = 0$ and system (40) becomes

$$\begin{aligned}
\frac{dz_1}{dN} &= -\alpha z_1z_2,\\
\frac{dz_2}{dN} &= -\frac{\alpha}{\alpha-1}z_1z_2.
\end{aligned} \tag{41}$$

Obviously, we can obtain $z_1 = (\alpha - 1)z_2 + C_1$, where C_1 is a constant. As z_1 is linearly related to z_2, the equilibrium point p_{10} is an unstable center when $\alpha > 1$ and a stable center when $\alpha < 0$ or $0 < \alpha < 1/2$ or $1/2 < \alpha < 1$.

Obviously, we can obtain $z_1 = (-1/2)z_2 + C_2$, where C_2 is a constant. As z_1 is linearly related to z_2, the equilibrium point q_9 is a stable center.

4. The Case $|\alpha| \to 1$ in 3D

According to Ref. [41], the best solution of this model can be achieved for α tending to one. Therefore, we present global phase of system (21) on three invariant planes when $|\alpha| \to 1$ in Figures 5 and 6, where CS represents the cosmological solution.

When $\alpha \to 1^-$, there is only one saddle matter point e_5 and one stable accelerated point e_4. The trajectory from e_5 to e_4 on the invariant plane $z = 0$ can be considered as a cosmological solution. However, this case approximates GR because $z = 0$ leads to $h(T) = 0$. Note that GR can not explain the late-time behavior of the universe. This cosmological solution is unacceptable.

When $\alpha \to 1^+$, e_4 is not an accelerated point, and e_6 is the only stable accelerated point instead. There is only one saddle matter point e_5. We can not find a cosmological solution on three invariant planes because the accelerated point e_6 and the matter saddle point e_5 are not on the same plane. However, by analyzing the trajectories around these three points in 3D, we find that the saddle matter point e_5 can reach the stable accelerated point e_6, which is an acceptable cosmological solution. This solution from e_5 to e_6 corresponds to the solution from P_3 to P_1 obtained in Ref. [41].

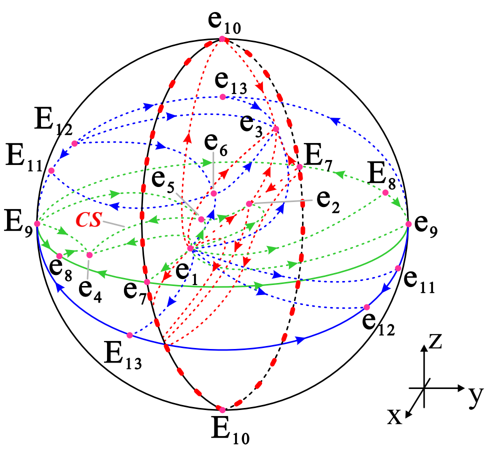

Figure 5. Phase portraits of system (21) on three invariant planes when $\alpha \to 1^-$.

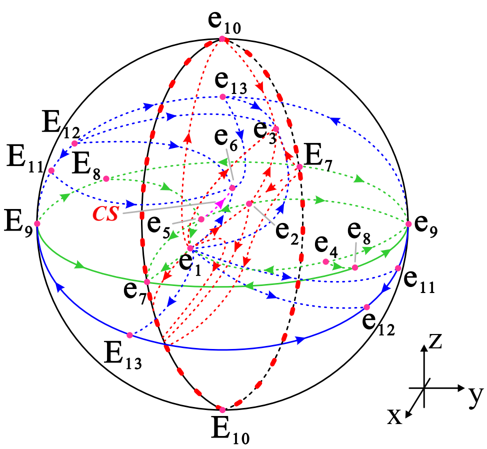

Figure 6. Phase portraits of system (21) on three invariant planes when $\alpha \to 1^+$.

5. The Form $g(R) = R + \xi R^{\alpha}$

In this section, we briefly discuss a case that is considered to be more interesting and physical when $f(R,T) = R + \xi R^{\alpha} + \zeta\sqrt{-T}$. Considering a spatially flat FLRW metric and the model's later-time behaviors. This theory gives

$$\begin{aligned} 1+&\frac{R+\xi R^{\alpha}}{6H^2(1+\xi\alpha R^{\alpha-1})}+\frac{\zeta\sqrt{-T}}{6H^2(1+\xi\alpha R^{\alpha-1})}-\frac{R}{6H^2}+\frac{\dot{g}'}{H(1+\xi\alpha R^{\alpha-1})} \\ &=\frac{8\pi G\rho^{(\mathrm{m})}}{3H^2(1+\xi\alpha R^{\alpha-1})}-\frac{\zeta\rho^{(\mathrm{m})}}{6H^2\sqrt{-T}(1+\xi\alpha R^{\alpha-1})}, \end{aligned} \tag{42}$$

and

$$\begin{aligned} 2&\frac{\dot{H}}{H^2}+\frac{\ddot{g}'}{H^2(1+\xi\alpha R^{\alpha-1})}-\frac{\dot{g}'}{H(1+\xi\alpha R^{\alpha-1})} \\ &=-\frac{8\pi G\rho^{(\mathrm{m})}}{H^2(1+\xi\alpha R^{\alpha-1})}+\frac{\zeta\rho^{(\mathrm{m})}}{2\sqrt{-T}H^2(1+\xi\alpha R^{\alpha-1})}, \end{aligned} \tag{43}$$

as the Friedmann-like equation and Raychaudhuri-like equation, respectively. The dynamical system becomes

$$\begin{aligned} \frac{dx_1}{dN} &= x_1(x_1-x_3)-3x_2-x_3-\frac{3}{2}x_4-1, \\ \frac{dx_2}{dN} &= \frac{x_1x_3}{m}+x_2(x_1-2x_3+4), \\ \frac{dx_3}{dN} &= -\frac{x_1x_3}{m}+2x_3(2-x_3), \\ \frac{dx_4}{dN} &= x_4\left(x_1-2x_3+\frac{5}{2}\right). \end{aligned} \tag{44}$$

The density parameter of matter $\Omega^{(\mathrm{m})}$ and effective equation of state $\omega^{(\mathrm{eff})}$ read as follows

$$\Omega^{(\mathrm{m})} = 1-x_1-x_2-x_3-x_4, \tag{45}$$

$$\omega^{(\mathrm{eff})} = \frac{1}{3}(1-2x_3). \tag{46}$$

The equilibrium points of system (44) and the related eigenvalues are listed in Tables 5 and 6, respectively. Furthermore, the parameter $r = r(x_2, x_3)$ satisfies

$$\frac{dr}{dN} = \frac{\partial r(x_2,x_3)}{\partial x_2}\frac{dx_2}{dN}+\frac{\partial r(x_2,x_3)}{\partial x_3}\frac{dx_3}{dN} = 0. \tag{47}$$

Using Equations (13)–(15), Equation (47) can be rewritten as

$$\frac{dr}{dN} = r\left(\frac{1+r+m(r)}{m(r)}\right)x_1 = 0, \tag{48}$$

where $m(r) = \alpha(r+1)/r$. Let

$$M(r) \equiv \frac{1+r+m(r)}{m(r)}, \tag{49}$$

which is well-defined for $m(r) \neq 0$ as all solutions that hold $m(r) = -r-1$ must satisfy $M(r) = 0$. Therefore, an acceptable solution must satisfy $r = 0$ or $M(r) = 0$ or $x_1 = 0$. By assuming $r \neq -1$ in Equation (49), we obtain $M(r) = 1 + r/\alpha$, which gives $M(r = -1) = 1 - 1/\alpha$. The condition $M(r) = 0$ is true only when $r = -\alpha$, resulting in

$m \neq 0$. On the other hand, the point q_6 is the matter point when $r = -1$. Note that models with $\alpha = 1$ can be acceptable, we mainly discuss the case of $\alpha \to 1$ where $M(r = -1) \approx 0$.

Table 5. Equilibrium points of system (44).

Equilibrium Points	Coordinates (x, y, z)	$\Omega^{(\mathrm{m})}$	$\omega^{(\mathrm{eff})}$
q_1	$(1, 0, 0, 0)$	0	$\frac{1}{3}$
q_2	$(-1, 0, 0, 0)$	2	$\frac{1}{3}$
q_3	$(-\frac{5}{2}, 0, 0, \frac{7}{2})$	0	$\frac{1}{3}$
q_4	$(-4, 5, 0, 0)$	0	$\frac{1}{3}$
q_5	$(0, -1, 2, 0)$	0	-1
q_6	$(\frac{3m}{m+1}, -\frac{4m+1}{2(1+m)^2}, \frac{4m+1}{2(m+1)}, 0)$	$\frac{2-3m-8m^2}{2(m+1)^2}$	$-\frac{m}{m+1}$
q_7	$(\frac{2(1-m)}{2m+1}, \frac{1-4m}{m(2m+1)}, -\frac{(1-4m)(m+1)}{m(2m+1)})$	0	$\frac{2-5m-6m^2}{3m(2m+1)}$
q_8	$(\frac{3m}{2(m+1)}, -\frac{8m+5}{4(m+1)^2}, \frac{8m+5}{4(m+1)}, \frac{4-3m-10m^2}{4(m+1)^2})$	0	$-\frac{2m+1}{2(m+1)}$

Table 6. Eigenvalues of equilibrium points.

Equilibrium Points	Eigenvalues
q_1	$\frac{7}{2}, 2, \frac{m(9m-1)+r(r+1)m'\pm a(m,m')}{2m^2}$
q_2	$-2, \frac{3}{2}, \frac{m(7m+1)-r(r+1)m'\pm a(m,m')}{2m^2}$
q_3	$-\frac{7}{2}, -\frac{3}{2}, \frac{m(11m+5)-r(r+1)m'\pm 5a(m,m')}{4m^2}$
q_4	$-5, -3, 4(1+\frac{1}{m}), -\frac{3}{2}$
q_5	$-3, -\frac{3}{2}, -\frac{3}{2} \pm \sqrt{\frac{25}{4} - \frac{4}{m}}$
q_6	$\frac{3}{2}, \frac{-3m\pm b(m)}{4m(m+1)}, 3(1+m')$
q_7	$\frac{1}{m}, \frac{-8m^2-3m+2}{m(2m+1)}, \frac{-4+2(1-m^2)(1+m')}{m(2m+1)}, \frac{-10m^2-3m+4}{2m(2m+1)}$
q_8	$-\frac{3}{2}, \frac{-3m(m+1)(2m+3)\pm c(m)}{8m(m+1)^2}, \frac{3}{2}(1+m')$

Note: $a(m,m') = \{m^2(m+1)^2 + rm'[-2m(m+1) + 2(m-1)mr + r(1+r^2)m']\}^{1/2}$, $b(m) \equiv [m(256m^3 + 160m^2 - 31m - 16)]^{1/2}$, $c(m) \equiv \{m(m+1)^2[m(676m^2 + 700m - 55) - 160]\}^{1/2}$.

When $\alpha \to 1^-$, as $r = -\alpha$, we can obtain $r \to -1^+$, which means $m(r) \to 0^+$. Within this range, the eigenvalues of point q_6 can be approximated as

$$\frac{3}{2}, \quad 3(1+m'), \quad -\frac{3}{4} \pm \sqrt{-\frac{1}{m}}. \tag{50}$$

This point is a matter saddle point with $\Omega^{(\mathrm{m})} = 1$ and $\omega^{(\mathrm{eff})} = 0$. The point q_8 is a stable accelerated point for $m'_{q_8} < -1$. Therefore, the transition from q_6 to q_8 is viable for leaving the matter-dominated era with $m'_{q_6} > -1$ and entering the accelerated epoch $m'_{q_8} < -1$. Moreover, the transition from q_6 to q_5 is possible. For $m(r = -2) = \alpha/2$, the de Sitter point q_5 is an acceptable final attractor for the cosmological solutions. When $m'_{q_6} > -1$, the trajectories can reach the final attractor q_5 after leaving the matter point q_6.

When $\alpha \to 1^+$, we obtain the limit $m(r) \to 0^-$. The point q_6 is not acceptable in this range because there are two eigenvalues approaching infinity. This indicates the matter-dominated era is short and does not match with the observational data. Since there are no other matter points, we cannot find the cosmological solution withinn this limit.

6. Conclusions

The dynamics of the $f(R, T)$ gravity model on the invariant planes for a perfect fluid in a spatially flat FLRW metric are studied with the form $g(R) + h(T)$. By considering the conservation of the energy–momentum tensor, it has been presented that the functionality of $h(T)$ must have the form $h(T) = C\sqrt{T}$ in the minimal models. More precisely, we mainly analyze the model in the type of $\xi R^{\alpha} + \zeta\sqrt{-T}$. We apply two powerful dynamic analysis tools, singularity theory, and Poincaré compactification. Using the singularity theory, we can understand the direction of trajectories near some unusual equilibrium points, such as saddle-nodes. The infinite phase space can be transformed into a finite space with the application of Poincaré compactification. Through the use of these two techniques, the stability of all the equilibrium points and global phase on the invariant planes is presented. Finally, we discussed the case of $|\alpha| \to 1$. All cosmological solutions have been marked in the figures.

Since the parameter α in this paper has a wider range of values, in order to accurately show the evolution of the model on three invariant planes simultaneously in space, we finally selected the limit $|\alpha| \to 1$, which visually illustrates the dynamic behavior of the model at this limit. The trajectory from e_5 to e_4 on the invariant plane $z = 0$ is not the desired cosmological solution when $\alpha \to 1^-$, and since this case approaches GR and we adopt it. When $\alpha \to 1^+$, we have a stable accelerated point e_6, and two saddle matter points e_2 and e_5. Although there are no cosmological solutions on the three invariant planes, by analyzing the trajectories around these three points, we find the trajectories from e_5 to e_6 exist, which can be considered as a cosmological solution. Furthermore, this solution is consistent with the cosmological solution from P_3 to P_4 in Ref. [41]. In addition, we briefly discuss a more interesting and physical form $f(R, T) = R + \xi R^{\alpha} + \zeta\sqrt{-T}$, and find two viable cosmological solutions q_6 to q_5 and q_6 to q_8 when $\alpha \to 1^-$.

Author Contributions: Conceptualization, F.G.; Formal analysis, J.L., R.W.; software, J.L.; writing—original draft, J.L.; writing—review and editing, F.G. All authors have read and agreed to the published version of the manuscript.

Funding: This research was funded by the National Natural Science Foundation of China (NSFC) through grant Nos. 12172322 and 11672259, the Postgraduate Research & Practice Innovation Program of Jiangsu Province (KYCX21_3190).

Institutional Review Board Statement: Not applicable.

Informed Consent Statement: Not applicable.

Data Availability Statement: Not applicable.

Acknowledgments: We are very grateful to the anonymous reviewers whose comments and suggestions helped improve and clarify this paper.

Conflicts of Interest: The authors declare no conflict of interest.

References

1. Will, C.M.; Anderson J.L. Theory and experiment in gravitational physics. *Am. J. Phys.* **1994**, *62*, 1153–1153. [CrossRef]
2. Turyshev, S.G. Experimental tests of general relativity: Recent progress and future directions. *Physics-Uspekhi* **2009**, *52*, 1. [CrossRef]
3. Iorio, L.; Lichteneggrr, H.I.M.; Ruggiero, M.L.; Corda, C. Phenomenology of the Lense-Thirring effect in the solar system. *Astrophys. Space. Sci.* **2011**, *331*, 351–395. [CrossRef]
4. Peeebles, P.J.E. Testing general relativity on the scales of cosmology. *arXiv* **2004**, arXiv:astro-ph/0410284.
5. Bennett, C.L.; Bay, M.; Halpern, M.; Hinshaw, G.; Jackson, C.; Jarosik, N.; Kogut, A.; Limon, M.; Meyer, S.S.; Page, L.; et.al. The microwave anisotropy probe* mission. *Astrophys. J.* **2003**, *583*, 1. [CrossRef]
6. Farajollahi, H.; Farhoudi, M.; Shojaie, H. On dynamics of Brans–Dicke theory of gravitation. *Int. J. Theor. Phys.* **2010**, *49*, 2558–2568. [CrossRef]
7. Bahrehbakhsh, A.F.; Farhoudi, M.; Shojaie, H. FRW cosmology from five dimensional vacuum Brans–Dicke theory. *Gen. Relativ. Gravit.* **2011**, *43*, 847–869. [CrossRef]
8. De Felice, A.; Tsujikawa, S. $f(R)$ Theories. *Living. Rev. Relativ.* **2010**, *13*, 3. [CrossRef]

9. Capozziello, S.; De Laurentis, M. Extended theories of gravity. *Phys. Rep.* **2011**, *509*, 167–321. [CrossRef]
10. Nojiri, S.; Odintsov, S.D. Mittal, A. Unified cosmic history in modified gravity: From $f(R)$ theory to Lorentz non-invariant models. *Phys. Rep.* **2011**, *505*, 59–144. [CrossRef]
11. Starobinsky, A.A. Disappearing cosmological constant in $f(R)$ gravity. *JETP. Lett.* **2007**, *86*, 157–163. [CrossRef]
12. Tsujikawa, S. Observational signatures of $f(R)$ dark energy models that satisfy cosmological and local gravity constraints. *Phys. Rev. D Part. Fields.* **2007**, 77, 315–317. [CrossRef]
13. Nojiri, S.; Odintsov, S.D.; Sáez-Gómez, D. Cosmological reconstruction of realistic modified $f(R)$ gravities. *Phys. Lett. B* **2009**, *681*, 74–80. [CrossRef]
14. Nojiri, S.; Odintsov, S.D.; Oikonomou, V.K. Unifying inflation with early and late-time dark energy in $f(R)$ gravity. *Phys. Dark Universe* **2020**, *29*, 100602. [CrossRef]
15. Hu, W.; Sawicki, I. Models of $f(R)$ cosmic acceleration that evade solar-system tests. *Astrophys. Space Sci.* **2007**, *76*, 064004. [CrossRef]
16. Bergliaffa, S.E.P. Constraining $f(R)$ theories with the energy conditions. *New Astron.* **2006**, *642*, 311–314.
17. Santos, J.; Alcaniz, J.S.; Reboucas, M.J.; Carvalho, F.C. Energy conditions in $f(R)$ gravity. *Phys. Rev. D* **2007**, *76*, 083513. [CrossRef]
18. Amendola, L.; Tsujikawa, S. Phantom crossing, equation-of-state singularities, and local gravity constraints in $f(R)$ models. *Phys. Lett. B* **2008**, *660*, 125–132. [CrossRef]
19. Pan, Y.; He, Y.; Qi, J.Z.; Li, J.; Cao, S.; Liu, T.H.; Wang, J. Testing $f(R)$ gravity with the simulated data of gravitational waves from the Einstein Telescope. *Astrophys. J.* **2021**, *911*, 135. [CrossRef]
20. Bertolami, O.; Boehmer, C.G.; Harko, T.; Lobo, F.S.N. Extra force in $f(R)$ modified theories of gravity. *Phys. Rev. D* **2007**, *75*, 104016. [CrossRef]
21. Harko, T. Modified gravity with arbitrary coupling between matter and geometry. *Phys. Lett. B* **2008**, *669*, 376–379. [CrossRef]
22. Harko T.; Lobo, F.S.N. $f(R, L_{\mathrm{m}})$ gravity. *Eur. Phys. J. C* **2010**, *70*, 373–379. [CrossRef]
23. Harko, T.; Lobo, F.S.N.; Nojiri, S.; Odintsov, S.D. $f(R, T)$ gravity. *Appl. Math. Nonlinear Sci.* **2011**, *84*, 024020. [CrossRef]
24. Sun, G.; Huang, Y.C. The cosmology in $f(R, \tau)$ gravity without dark energy *Int. J. Mod. Phys. D* **2016**, *25*, 1650038. [CrossRef]
25. Zaregonbadi, R.; Farhoudi, M.; Riazi, N. Dark matter from $f(R, T)$ gravity. *Phys. Rev. D* **2016**, *94*, 084052. [CrossRef]
26. Bhattacharjee, S.; Sahoo, P.K. Redshift drift in $f(R, T)$ gravity. *New Astron.* **2020**, *81*, 101425. [CrossRef]
27. Moraes, P.H.R.S.; Sahoo, P.K. Nonexotic matter wormholes in a trace of the energy-momentum tensor squared gravity. *Phys. Rev. D* **2018**, *57*, 024007. [CrossRef]
28. Bhatti, M.Z.; Yousaf, Z.; Ilyas, M. Existence of wormhole solutions and energy conditions in $f(R, T)$ gravity. *J. Astrophys.* **2018**, *39*, 1–11. [CrossRef]
29. Sharif, M.; Zubair, M. Thermodynamics in $f(R, T)$ theory of gravity. *J. Cosmol. Astropart. Phys.* **2012**, *2012*, 028. [CrossRef]
30. Houndjo, M.J.S.; Alvarenga, F.G.; Rodrigues, M.E.; Jardim, D.F.; Myrzakulov, R. Thermodynamics in Little Rip cosmology in the framework of a type of $f(R, T)$ gravity. *Eur. Phys. J. Plus* **2014**, *129*, 1–12. [CrossRef]
31. Bhattacharjee, S.; Sahoo, P.K. Comprehensive analysis of a non-singular bounce in $f(R, T)$ gravitation. *Phys. Dark Universe* **2020**, *28*, 100537. [CrossRef]
32. Sahoo, P.; Bhattacharjee, S.; Tripathy, S.K.; Sahoo, P.K. Bouncing scenario in $f(R, T)$ gravity. *Mod. Phys. Lett. A* **2020**, *35*, 2050095. [CrossRef]
33. Sahoo, P.K.; Bhattacharjee, S. Gravitational baryogenesis in non-minimal coupled $f(R, T)$ gravity. *Int. J. Theor. Phys.* **2020**, *59*, 1451–1459. [CrossRef]
34. Alvarenga, F.G.; De La Cruz-Dombriz, A.; Houndjo, M.J.S.; Rodrigues, M.E.; Sáez-Gómez, D. Dynamics of scalar perturbations in $f(R, T)$ gravity. *Phys. Rev. D* **2013**, *87*, 103526. [CrossRef]
35. Alves, M.E.S.; Moraes, P.H.R.S.; De Araujo, J.C.N.; Malheiro, M. Gravitational waves in $f(R, T)$ and $f(R, T\phi)$ theories of gravity. *Phys. Rev. D* **2016**, *94*, 024032. [CrossRef]
36. Sharif, M.; Siddiqa, A. Propagation of polar gravitational waves in $f(R, T)$ scenario. *Gen. Relativ. Gravit.* **2019**, *51*, 74. [CrossRef]
37. Houndjo, M.J.S. Reconstruction of $f(R, T)$ gravity describing matter dominated and accelerated phases. *Int. J. Mod. Phys. D* **2012**, *21*, 1250003. [CrossRef]
38. Sharif, M.; Zubair, M. Cosmological reconstruction and stability in $f(R, T)$ gravity. *Gen. Relativ. Gravit.* **2014**, *46*, 1723. [CrossRef]
39. Singh, C.P.; Singh, V. Reconstruction of modified $f(R, T)$ gravity with perfect fluid cosmological models. *Gen. Relativ. Gravit.* **2014**, *46*, 1696. [CrossRef]
40. Shabani, H.; Farhoudi, M. Cosmological and solar system consequences of $f(R, T)$ gravity models. *Phys. Rev. D* **2014**, *90*, 044031. [CrossRef]
41. Shabani, H.; Farhoudi, M. $f(R, T)$ cosmological models in phase space. *Phys. Rev. D* **2013**, *88*, 044048. [CrossRef]
42. Baffou, E.H.; Kpadonou, A.V.;Rodrigues, M.E.; Houndjo, M.J.S.; Tossa, J. Cosmological viable $f(R, T)$ dark energy model: Dynamics and stability. *Astrophys. Space. Sci.* **2015**, *356*, 173–180. [CrossRef]
43. Sharma, U.K.; Pradhan, A. Propagation of polar gravitational waves in $f(R, T)$ scenario. *Int. J. Geom. Methods Mod. Phys.* **2018**, *15*, 1850014. [CrossRef]
44. Abchouyeh, M.A.; Mirza, B.; Shahidi, P.; Oboudiat, F. Late time dynamics of $f(R, T, R_{\mu\nu}T^{\mu\nu})$ gravity. *Int. J. Geom. Methods Mod. Phys.* **2020**, *17*, 2050008. [CrossRef]

45. Gonçalves, T.B.; Rosa, J.L.; Lobo, F.S.N. Cosmology in the novel scalar-tensor representation of $f(R,T)$ gravity. *arXiv* **2021**, arXiv:2112.03652.
46. Santos, A.F. Gödel solution in $f(R,T)$ gravity. *Mod. Phys. Lett. A* **2013**, *28*, 1350141. [CrossRef]
47. Guo, J.Q.; Frolov, A.V. Cosmological dynamics in $f(R)$ dravity. *Phys. Rev. D* **2013**, *88*, 124036. [CrossRef]
48. Zonunmawia, H; Khyllep, W; Dutta, J; Järv, L. Cosmological dynamics of brane gravity: A grobal dynamical system perspective. *Phys. Rev. D* **2018**, *98*, 083532. [CrossRef]
49. Gao, F.B.; Llibre, J. Global dynamics of the Hořava-Lifshitz cosmological model in a non-flat universe with non-zero cosmological constant. *Universe* **2021**, *7*, 445. [CrossRef]
50. Singh, A.; Singh, G.P.; Pradhan A. Cosmic dynamics and qualitative study of Rastall model with spatial curvature. *arXiv* **2022**, arXiv:2205.13934.
51. Amendola, L. Coupled quintessence. *Phys. Rev. D* **2000**, *62*, 043511. [CrossRef]
52. Dumortier, F.; Llibre, J.; Ateés, J.C. *Qualitative Theory of Planar Differential Syetems*; Springer: Berlin/Heidelberg, Germany, 2006.
53. Cima, A.; Llibre, J. Bounded polynomial vector fields. *Trans. Am. Math. Soc.* **1990**, *318*, 557–579. [CrossRef]
54. Álvarez, M.J.; Pugh, C.C.; Shub, M. *Invariant Manifolds*; Springer: Berlin/Heidelberg, Germany, 1977.